Primary cilia control translation and the cell cycle in medulloblastoma

Yong Ha Youn,[1] Shirui Hou,[1] Chang-Chih Wu,[1] Daisuke Kawauchi,[2] Brent A. Orr,[3] Giles W. Robinson,[4] David Finkelstein,[5] Makoto M. Taketo,[6] Richard J. Gilbertson,[7] Martine F. Roussel,[8] and Young-Goo Han[1]

[1]Department of Developmental Neurobiology, St. Jude Children's Research Hospital, Memphis, Tennessee 38105, USA; [2]Department of Biochemistry and Cellular Biology, National Center of Neurology and Psychiatry, Tokyo 187-8551, Japan; [3]Department of Pathology, St. Jude Children's Research Hospital, Memphis, Tennessee 38105, USA; [4]Division of Neuro-Oncology, Department of Oncology, St. Jude Children's Research Hospital, Memphis, Tennessee 38105, USA; [5]Department of Computational Biology, St. Jude Children's Research Hospital, Memphis, Tennessee 38105, USA; [6]Graduate School of Medicine, Kyoto University, Kyoto 606-8501, Japan; [7]Department of Oncology, Cancer Research UK Cambridge Institute, Cambridge CB2 0RE, England; [8]Department of Tumor Cell Biology, St. Jude Children's Research Hospital, Memphis, Tennessee 38105, USA

The primary cilium, a signaling organelle projecting from the surface of a cell, controls cellular physiology and behavior. The presence or absence of primary cilia is a distinctive feature of a given tumor type; however, whether and how the primary cilium contributes to tumorigenesis are unknown for most tumors. Medulloblastoma (MB) is a common pediatric brain cancer comprising four groups: SHH, WNT, group 3 (G3), and group 4 (G4). From 111 cases of MB, we show that primary cilia are abundant in SHH and WNT MBs but rare in G3 and G4 MBs. Using WNT and G3 MB mouse models, we show that primary cilia promote WNT MB by facilitating translation of mRNA encoding β-catenin, a major oncoprotein driving WNT MB, whereas cilium loss promotes G3 MB by disrupting cell cycle control and destabilizing the genome. Our findings reveal tumor type-specific ciliary functions and underlying molecular mechanisms. Moreover, we expand the function of primary cilia to translation control and reveal a molecular mechanism by which cilia regulate cell cycle progression, thereby providing new frameworks for studying cilium function in normal and pathologic conditions.

[*Keywords*: cell cycle; cilia; medulloblastoma; translation; WNT]

Supplemental material is available for this article.

Received March 24, 2022; revised version accepted June 17, 2022.

The primary cilium plays important roles in multiple signaling pathways, whose dysfunctions contribute to tumorigenesis (Eguether and Hahne 2018; Liu et al. 2018). The cilium grows from the basal body, a modified centriole, anchored to the cell membrane. Before undergoing mitosis, a cell must disassemble its cilium to convert the basal body into the centrosome that organizes the mitotic spindle. Thus, cell cycle progression is tightly associated with the assembly and disassembly of primary cilia (Izawa et al. 2015; Wang and Dynlacht 2018). Notably, the presence or absence of primary cilia is a distinctive feature of many tumor types and of tumor stages in some tumors (Eguether and Hahne 2018; Liu et al. 2018). Moreover, cilium gain or loss during targeted therapy can render tumor cells resistant to such therapies (Zhao et al. 2017; Jenks et al. 2018). These observations suggest that primary cilia play important roles in the development and progression of diverse tumors and that these roles differ between tumor types. A mechanistic understanding of the function of cilia in the context of each tumor type will provide insights into tumorigenic mechanisms and reveal new therapeutic targets.

Medulloblastoma (MB) is the most common malignant brain tumor in children. It comprises four groups: SHH, WNT, group 3 (G3), and group 4 (G4), which show distinct molecular, pathologic, and clinical features (Wang et al. 2018; Juraschka and Taylor 2019; Northcott et al. 2019). SHH and WNT MBs are driven by abnormally active SHH and WNT signaling, respectively. For G3 and G4 MBs, no common driver pathways have been identified other than recurrent *MYC* amplification, which is present in 17% of G3 MBs. Despite the distinct features of the different MB groups, patients with MB receive largely identical treatments: surgical resection, cytotoxic chemotherapy, and radiation therapy. Current therapies fail to cure one-third of

Corresponding author: young-goo.han@stjude.org
Article published online ahead of print. Article and publication date are online at http://www.genesdev.org/cgi/doi/10.1101/gad.349596.122. Freely available online through the *Genes & Development* Open Access option.

patients, and survivors experience lifelong, debilitating side effects. Radiation and chemotherapy can also cause secondary malignancies. Therefore, we need a deeper understanding of the mechanisms that drive each MB type in order to develop specific, effective, and less toxic therapies.

Early evidence for the tumor-specific roles of primary cilia came from studies in basal cell carcinoma and MB driven by SHH signaling (Han et al. 2009; Wong et al. 2009). Primary cilia are required or inhibitory for SHH MB, depending on the tumor-initiating mutations. In mice, constitutively active Smoothened, an upstream activator of SHH signaling, requires primary cilia in order to induce SHH MB; however, constitutively active GLI2, a transcription factor downstream from SHH signaling, requires cilium loss to induce SHH MB. Primary cilia play similar dual opposing roles in basal cell carcinoma. Notably, primary cilia are abundant in SHH and WNT MB but rare in the other groups (Han et al. 2009). Nevertheless, it is unknown whether primary cilia play a role in MB groups other than SHH MB. Here, we report that primary cilia promote WNT MB but inhibit G3 MB. Mechanistically, primary cilia promoted WNT MB by facilitating the synthesis of β-catenin, the major oncoprotein driving WNT MB, whereas cilium loss promoted G3 MB by abnormally activating cyclin-dependent kinase 1 (CDK1), disrupting cell cycle control, and increasing genome instability. Our studies reveal novel functions of primary cilia in translation and cell cycle progression, fundamental processes commonly misappropriated for tumorigenesis.

Results

Association of primary cilia with distinct human MB groups

We previously showed that primary cilium prevalence is tightly associated with the molecular groups of human MB in a cohort of 24 samples (Han et al. 2009). To verify these initial findings obtained from a small number of samples, we quantified primary cilia in 111 human MB samples comprising 22 SHH, 13 WNT, nine G3, and 23 G4 samples and 44 samples defined as non-WNT/non-SHH (NWNS). Consistent with the previous observation, primary cilia were abundant in SHH and WNT MBs but rare in the other groups (Fig. 1A,B).

SHH MBs showed considerable variation in cilium frequency. Notably, seven *GLI2*-amplified SHH MB samples had significantly fewer cilia than did the other 15 SHH MB samples without *GLI2* amplifications (Fig. 1A,C). The *GLI2*-amplified MB with the highest frequency of ciliated cells had bulged cilia, a sign of defective ciliogenesis (see below). These results suggest that ciliogenesis in *GLI2*-amplified MBs is impaired. Previously, we showed that primary cilia suppress GLI2-driven MB development and must be removed for GLI2 to induce MB in mice (Han et al. 2009). Similarly, primary cilia might inhibit GLI2-driven SHH MB in humans; however, more *GLI2*-amplified MBs need to be examined before a definitive conclusion can be drawn about this. In our SHH MB cohort, 16 samples were verified as *TP53* wild type and three as *TP53* mutant. The cilia frequencies did not differ significantly between the *TP53* wild-type and mutant samples (Fig. 1D). The three *TP53* mutant SHH MBs included the sample that had the highest frequency of ciliated cells and two samples that had the lowest frequency of ciliated cells, which had *GLI2* amplification. Although more *TP53* mutant SHH MBs should be examined, these initial findings suggest that *TP53* mutation status is not associated with cilium frequency in SHH MBs.

In two of 22 SHH MB samples, the cilia appeared bulged (Fig. 1A, inset and arrows). Bulged cilia form when ciliary components accumulate abnormally at the tip of the cilia as a result of defective retrograde intraflagellar transport (IFT), a dedicated trafficking mechanism inside cilia (Rosenbaum and Witman 2002; Taschner and Lorentzen 2016). Defective retrograde IFT can cause hyperactivation of hedgehog signaling (Tran et al. 2008; Stottmann et al. 2009; Mukhopadhyay et al. 2010; Qin et al. 2011); therefore, the abundant bulged cilia in two SHH MB samples suggest that defective retrograde IFT contributes to the hyperactivation of SHH signaling in these MBs.

Primary cilia are present in WNT MBs but absent in G3 MBs in mouse models

Primary cilium prevalence was tightly associated with the molecular groups of human MB (Fig. 1). Remarkably, in mouse models, primary cilia were also present in WNT MBs driven by a constitutively active β-catenin and a constitutively active PI3 kinase [*Blbp::Cre; Ctnnb*$^{loxp(ex3)/+}$; *Pik3ca*$^{loxp(E545K)/+}$] (Robinson et al. 2012) but absent in G3 MBs developed from orthotopically implanted *Trp53*$^{-/-}$ cerebellar granule neuron precursor cells (GNPs) overexpressing MYC (Fig. 1E; Kawauchi et al. 2012). These findings, together with previous ones that primary cilia promote or suppress SHH MB in mice depending on the tumor-initiating mutation, suggest that primary cilia play distinct and critical roles in WNT and G3 MB.

Primary cilium loss in mouse WNT MB inhibits tumor development

To investigate the role of primary cilia in WNT MB, we removed primary cilia from WNT MBs by conditionally deleting *Kif3a*, a gene essential for ciliogenesis (Marszalek et al. 1999, 2000), in *Blbp::Cre; Ctnnb1*$^{fl(ex3)/+}$; *Pik3ca*$^{fl(E545K)/+}$; *Kif3a*$^{fl/fl}$ mice. Remarkably, cilium loss blocked WNT MB formation in one-third of the mice and delayed tumor development in the others, significantly extending the life span of tumor-bearing mice (Fig. 2A–C). WNT MB develops from ectopically accumulated cells in the dorsal brainstem (Gibson et al. 2010). This ectopic cell accumulation still formed in the absence of cilia (Fig. 2D). All control WNT MB mice [*Blbp::Cre; Ctnnb1*$^{fl(ex3)/+}$; *Pik3ca*$^{fl(E545K)/+}$; *Kif3a*$^{fl/+}$] succumbed to their tumors within 200 d after birth. In contrast, more than half of the mice lacking cilia [*Blbp::Cre; Ctnnb1*$^{fl(ex3)/+}$; *Pik3ca*$^{fl(E545K)/+}$; *Kif3a*$^{fl/fl}$] remained alive at 200 d after birth (Fig. 2C), and the ectopically clustered cells in those mice that had not developed tumors had

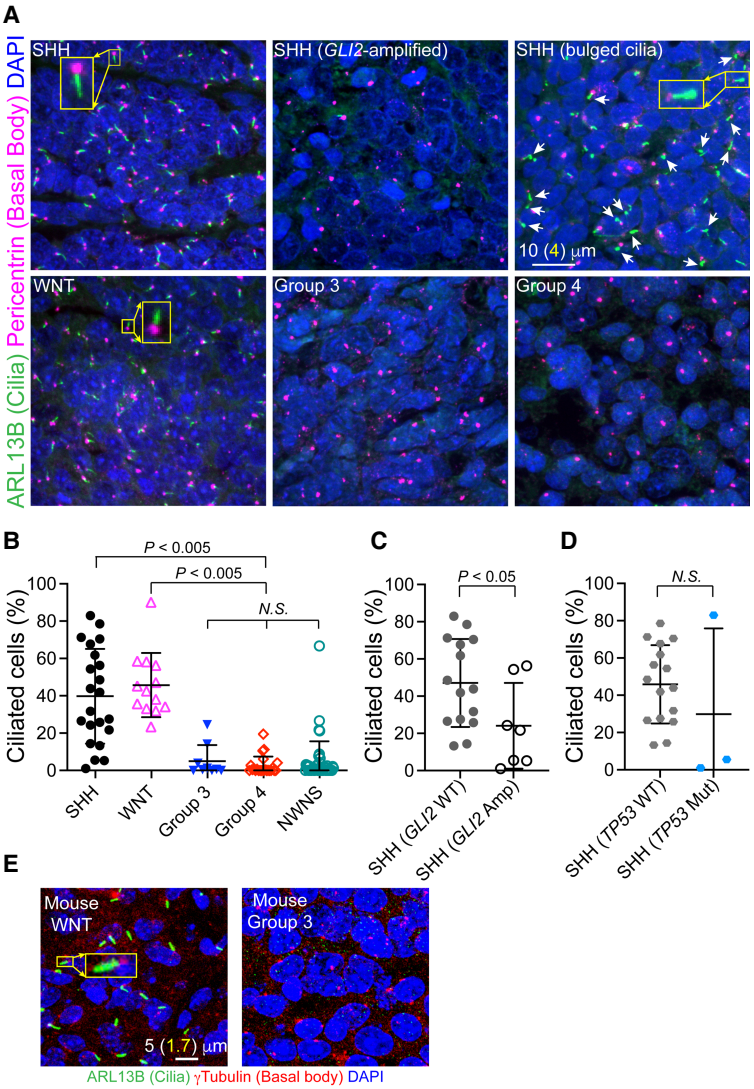

Figure 1. Prevalence of primary cilia in human and mouse MBs. (*A*) Primary cilia were abundant in SHH and WNT MBs but rare in other MBs. Primary cilia were stained with an antibody to ARL13B (green), basal bodies were stained with an antibody to pericentrin (magenta), and nuclei were stained with DAPI (blue). The *top* row shows examples of SHH MBs, including a *GLI2*-amplified MB and an MB containing abundant bulged cilia (white arrows). The *bottom* row shows examples of tumors from the other MB groups. (*B*) Quantification of ciliated cells in human MBs (mean ± standard deviation [SD], Kruskal–Wallis test with Dunn's multiple comparison test). (*C*,*D*) Quantification of ciliated cells in SHH MBs with respect to *GLI2* amplification (*C*) and *TP53* mutation (*D*) (mean ± SD, Mann–Whitney test). (*E*) In mouse models, primary cilia were present in WNT MBs but not in G3 MBs. Primary cilia are stained green (ARL13B), basal bodies are stained red (γ-tubulin), and nuclei are stained blue (DAPI). *Insets* are high-magnification images.

many apoptotic cells and no proliferating cells (Fig. 2E). Therefore, primary cilia were required to enhance the proliferation and survival of the cells of origin of WNT MB. The WNT MBs that formed without cilia also showed decreased proliferation and increased cell death when compared with control WNT MBs (Fig. 2F).

Transformed WNT MB cells require primary cilia for survival and proliferation

Our data showed that primary cilia are required for the development of WNT MB from the ectopically accumulated cells of origin. Fully transformed WNT MB cells maintained primary cilia (Fig. 1). To investigate whether primary cilia were still required by the fully transformed WNT MB cells, we transduced primary WNT MB cells isolated from WNT MB mice with lentiviruses expressing control shRNAs (shCTL) or shRNAs targeting *Ift88* (shIft88), an essential ciliogenic gene (Pazour et al. 2000). We chose to knock down *Ift88* instead of *Kif3a* to confirm that the effect of *Kif3a* loss was due to cilium loss. WNT MB cells were also transduced with lentiviruses expressing luciferase to monitor tumor growth. The implanted tumor cells formed secondary tumors that had primary cilia (Fig. 3A). Acute removal of cilia by shIft88 from primary WNT MB cells significantly delayed secondary tumor development and prolonged the survival of tumor-bearing mice (Fig. 3A–C). The loss of either *Kif3a* or *Ift88*, two different ciliogenic genes, similarly impeded WNT MB growth, supporting the hypothesis that cilia promote WNT MB growth. Similar to the chronic cilium loss in the cells of origin of WNT MB (Fig. 2F), acute cilium loss in fully transformed WNT MB increased cell death and decreased proliferation (Fig. 3D). Furthermore, cilium loss significantly decreased the proportion of cells re-entering the cell cycle and increased the proportion exiting it (Fig. 3E), as assessed by sequential labeling with two thymidine analogs, BrdU and EdU, that were injected at 24 and 2 h, respectively, before euthanasia. Consistently, cilium loss strongly increased the number of cells expressing the differentiated neuronal marker TUJ1 in

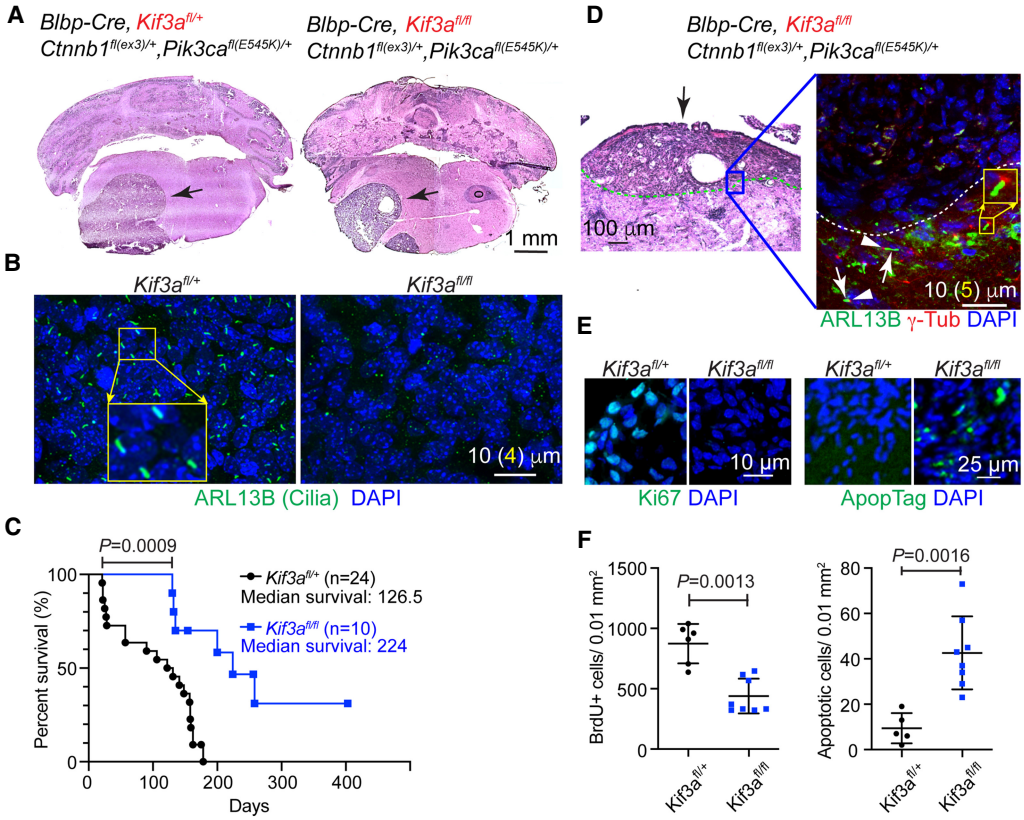

Figure 2. Primary cilium loss inhibits WNT MB development. (*A*) H&E staining showing WNT MB in the brainstem (arrows). (*B*) WNT MB sections stained for primary cilia (ARL13B, green) and nuclei (DAPI, blue). Cilia were present in control WNT MB (*Kif3a*$^{fl/+}$) but not in *Kif3a*$^{fl/fl}$ mutant WNT MB. (*C*) Survival curve showing that cilium loss (*Kif3a*$^{fl/fl}$) in WNT MB prolonged survival of mice (log-rank test). (*D*) H&E staining showing an ectopic cluster of cells (*left* panel, arrow) formed in the dorsal brainstem in the absence of cilia (*Kif3a*$^{fl/fl}$). Dotted lines demarcate the ectopic cluster. The *right* panel shows that primary cilia were present outside the ectopic cluster but not within it. Primary cilia are stained green (ARL13B), basal bodies are stained red (γ-tubulin), and nuclei are stained blue (DAPI). (*E*) Ectopic clusters stained for markers of proliferation (Ki67, green) and apoptosis (ApopTag, green) showed apoptotic cells but no proliferating cells in the absence of cilia. (*F*) Quantification of BrdU$^+$ cells and apoptotic cells in control (*Kif3a*$^{fl/+}$) and *Kif3a*$^{fl/fl}$ mutant WNT MBs (mean ± SD, Mann–Whitney test). *Insets* are high-magnification images.

WNT MB (Fig. 3F). Therefore, fully transformed WNT MB cells still required primary cilia for optimal survival and continuous proliferation.

Loss of cilia decreases β-catenin-dependent transcription

To understand the mechanism by which cilium loss inhibited WNT MB, we sequenced RNA from shCTL WNT MB and shIft88 WNT MB. Ingenuity Pathway Analysis (IPA) of RNA-seq data revealed β-catenin to be the most significantly inhibited upstream regulator ($P = 3.06 \times 10^{-7}$) (Supplemental Fig. S1A). RT-qPCR of WNT MB target genes confirmed that β-catenin target gene expression was decreased in shIft88 WNT MB as compared with shCTL WNT MB (Fig. 4A). The expression level of *Axin2*, a well-known transcriptional target of WNT signaling, was not decreased by cilium loss, suggesting that the decreased β-catenin activity in cilium-deficient tumor cells was still sufficient to activate expression of some β-catenin target genes.

Cilium loss decreases β-catenin synthesis

To understand why β-catenin target gene expression was decreased in tumor cells lacking cilia, we examined the β-catenin levels. Cilium loss dramatically decreased β-catenin protein levels, especially in nuclei (Fig. 4B,C), but not mRNA levels (Supplemental Fig. S1B,C), in WNT MB. Cilium loss also decreased β-catenin protein levels in primary WNT MB cells in culture (Fig. 4D,G). β-Catenin levels in cells transduced with shCTL and in nontransduced WNT MB cells (WT) were similar, indicating that lentiviral transduction of shRNAs per se did not affect β-catenin protein levels (Fig. 4D). The decrease in β-catenin protein levels but not mRNA levels was surprising because *Ctnnb1*$^{fl(ex3)/+}$ in our WNT MB mouse model encodes a mutant β-catenin that is resistant to phosphorylation and ubiquitin-mediated degradation (Harada et al. 1999). Therefore, we examined whether cilium loss affected β-catenin protein synthesis. To assess the β-catenin synthesis rate, we blocked protein synthesis with low-dose cycloheximide for 16 h and then removed the cycloheximide

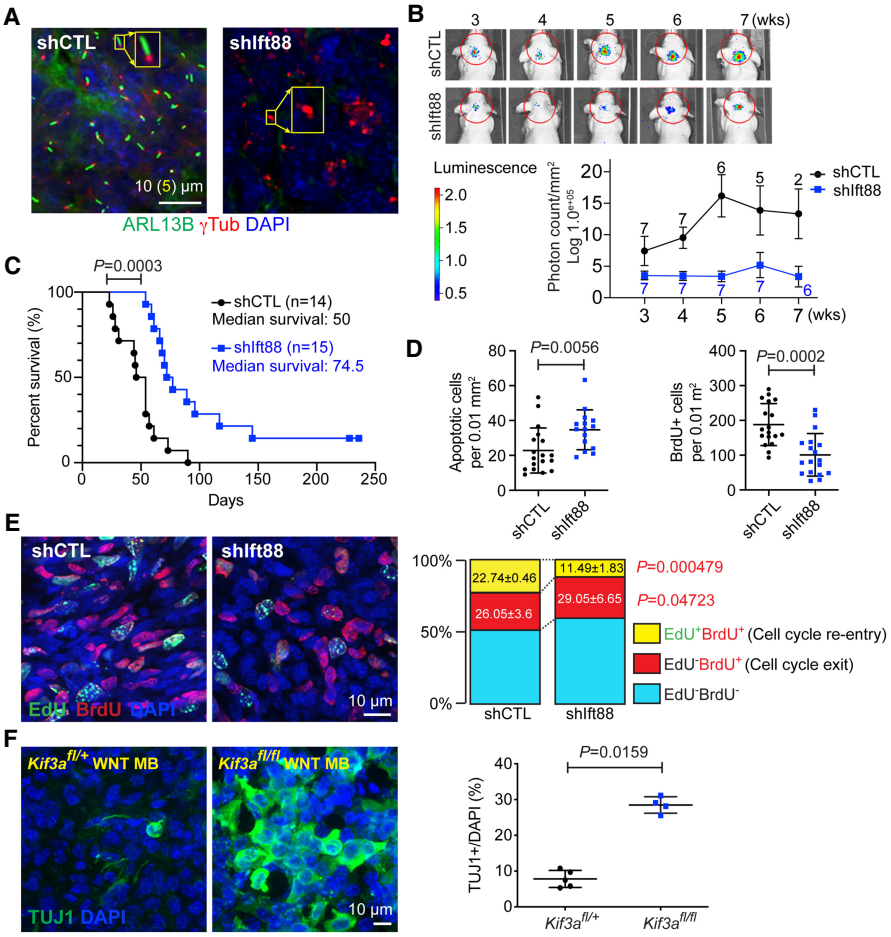

Figure 3. Primary cilia promote proliferation and survival of WNT MB cells. (*A*) Immunofluorescence images of secondary WNT MB formed from implanted WNT MB cells transduced with lentiviruses expressing shCTL or shIft88 shRNA. Cilia are stained green (ARL13B), basal bodies are stained red (γ-tubulin), and nuclei are stained blue (DAPI). *Insets* are high-magnification images. (*B*) Bioluminescence images and quantifications of implanted WNT MB cells expressing luciferase. The numbers *above* and *below* the plots are the number of animals per time point. (*C*) Survival curves showing that cilium loss (shIft88) in WNT MB cells prolonged the survival of tumor-implanted mice (log-rank test). (*D*) Quantification of BrdU$^+$ and apoptotic cells in secondary WNT MBs with cilia (shCTL) or without cilia (shIft88) (mean ± SD, unpaired *t*-test). (*E*) WNT MB sections stained for BrdU (red) and EdU (green), which were injected 24 and 1 h, respectively, before the mice were euthanized, and quantifications (mean ± SD, unpaired *t*-test). (*F*) WNT MB sections stained for TUJ1 (green) and quantifications (mean ± SD, Mann–Whitney test).

in the presence of MG132, a proteasome inhibitor, so that newly synthesized β-catenin proteins could accumulate and be assessed over time. Upon removal of cycloheximide, β-catenin protein levels increased gradually in control cells; however, this increase was severely blunted in cells lacking cilia (Fig. 4E,F). We independently performed this experiment twice. Although the combined results from the two experiments were not statistically significant because of relatively high variability in shCTL cells between the two experiments, cilium loss strongly decreased β-catenin synthesis in each experiment.

Cilium loss disrupts localization of ELAVL1, which promotes β-catenin synthesis

To investigate how cilium loss decreased β-catenin protein synthesis, we examined ELAVL1, an RNA binding protein that binds to β-catenin mRNA and regulates its translation (Peng et al. 1998; López de Silanes et al. 2003; Cao et al. 2015; Chou et al. 2015; Palomo-Irigoyen et al. 2020; Schultz et al. 2020). Cilium loss drastically changed the distribution of ELAVL1. ELAVL1 was distributed throughout cells in control WNT MBs but accumulated in the nuclei of WNT MB cells lacking cilia both in vivo and in vitro (Fig. 4G,H). Importantly, cytoplasmic, but not nuclear, ELAVL1 promotes translation of its target mRNAs (Atasoy et al. 1998; Fan and Steitz 1998; Peng et al. 1998; Wang et al. 2000; Grammatikakis et al. 2017; Schultz et al. 2020). We knocked down ELAVL1 to test whether it controlled β-catenin protein synthesis in WNT MB cells. ELAVL1 knockdown decreased the levels and synthesis of β-catenin in WNT MB cells in a manner similar to cilium loss (Fig. 4D–F), indicating that ELAVL1 promotes β-catenin protein synthesis in WNT MB.

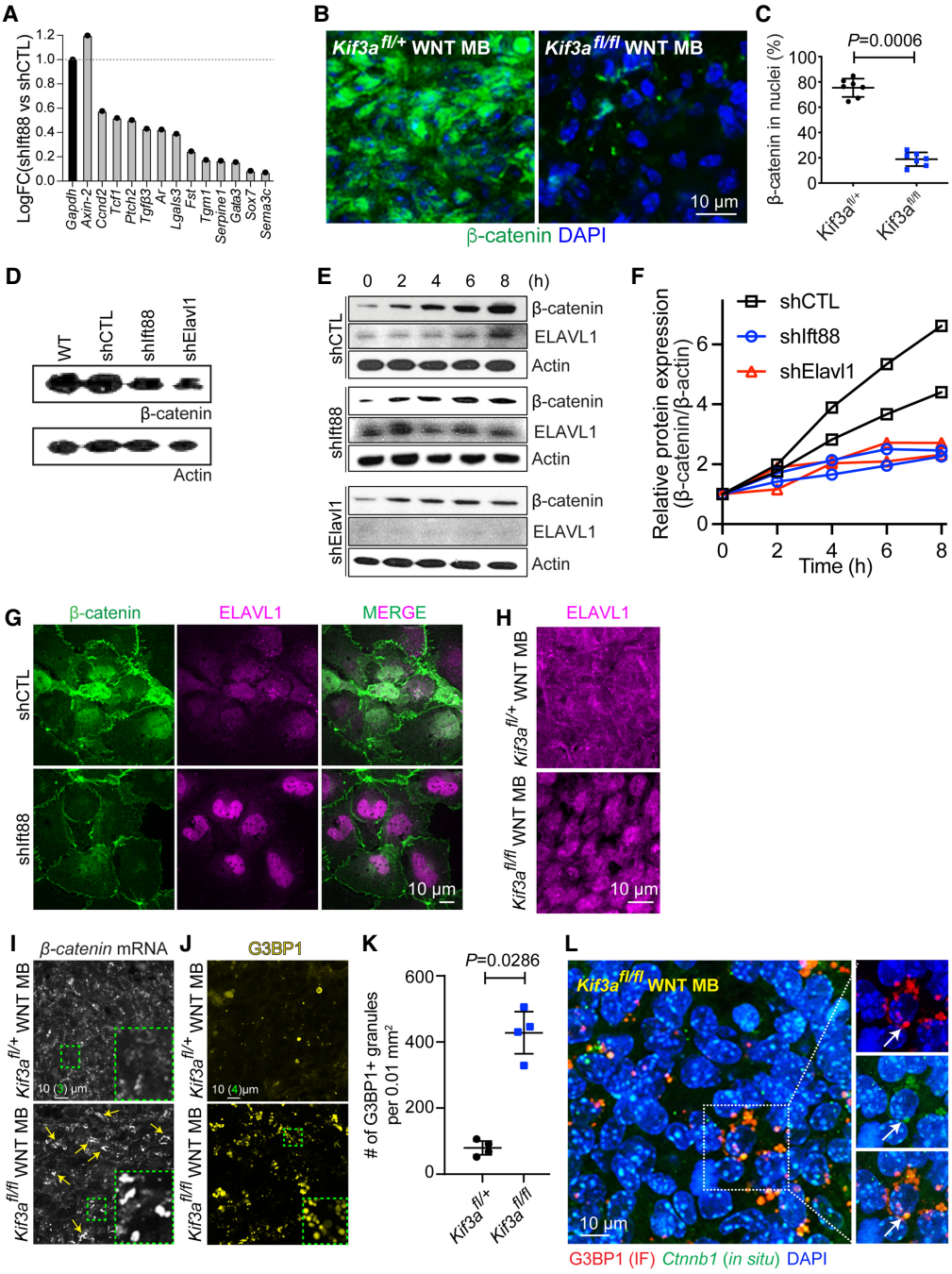

Figure 4. Primary cilia promote β-catenin mRNA translation in WNT MB cells. (*A*) Cilium loss decreased β-catenin target mRNA levels in WNT MB. The bars show the fold changes in *Gapdh*-normalized mRNA levels relative to those in control WNT MB (shCTL) as measured by qPCR. (*B*,*C*) Cilium loss decreased nuclear β-catenin (green) in WNT MB. Plots show the mean ± SD (Mann–Whitney test). (*D*) Western blot showing that knockdown of cilia (shIft88) or of ELAVL1 decreased β-catenin levels in WNT MB cells in culture. (*E*,*F*) Loss of cilia or of ELAVL1 decreased β-catenin protein synthesis in WNT MB cells. Western blots (*E*) and quantifications (*F*) show gradual accumulation of β-catenin after cells are released from translation block by cycloheximide. The graphs show results from two independent experiments. (*G*) Cilium loss (shIft88) decreased nuclear β-catenin (green) and increased nuclear ELAVL1 levels in WNT MB cells in culture. (*H*) ELAVL1 (magenta) distributed throughout a cell in control (*Kif3a*$^{fl/+}$) WNT MB in vivo. Cilium loss (*Kif3a*$^{fl/fl}$) induced nuclear accumulation of ELAVL1 in WNT MB cells in vivo. (*I*) Fluorescent in situ hybridization signal shows β-catenin mRNA distribution. A weak, gray in situ hybridization signal was diffused throughout the control WNT MB tumor (*Kif3a*$^{fl/+}$) but was absent in WNT MBs lacking cilia (*Kif3a*$^{fl/fl}$), in which the hybridization signal formed large aggregates (arrows). *Insets* are high-magnification images. (*J*,*K*) Cilium loss (*Kif3a*$^{fl/fl}$) increased granules labeled with the G3BP1 antibody in WNT MB. Plots show the mean ± SD (Mann–Whitney test). (*L*) Immunofluorescence combined with in situ hybridization shows colocalization of G3BP1 protein (red) and β-catenin mRNA (green) in granules. The arrow indicates an example of colocalization.

Nuclear accumulation of ELAVL1 may contribute to impaired β-catenin synthesis in WNT MB cells lacking cilia.

Cilium loss increases G3BP1$^+$ granules containing β-catenin mRNA

The mislocalization of ELAVL1 prompted us to examine β-catenin mRNA localization. Fluorescent in situ hybridization (FISH) showed that β-catenin mRNA was distributed throughout the cytoplasm (the weak and diffuse gray signal in Fig. 4I, top panel) and formed small speckles in control WNT MB cells. Remarkably, β-catenin mRNA aggregated to large bodies in WNT MB cells lacking primary cilia (Fig. 4I). The diffuse gray FISH signal for β-catenin mRNA in control WNT MB cells largely disappeared in WNT MB cells lacking cilia (the images were acquired using the same acquisition settings and were not subsequently modified). The aggregated β-catenin mRNA in the WNT MB cells lacking cilia was reminiscent of stress granules, which form from mRNAs stalled in translation initiation (Kedersha et al. 2013; Protter and Parker 2016). Indeed, cilium loss strongly increased granules marked by G3BP1, a canonical marker and a key nucleating protein of stress granules (Fig. 4J,K). Furthermore, G3BP1 and β-catenin mRNA colocalized in the granules (Fig. 4L), suggesting that cilium loss increased stress granules containing β-catenin mRNA whose translation was disrupted. Together, our results show that primary cilia promote WNT MB by facilitating the synthesis of β-catenin, the major oncogenic driver in 90% of WNT MBs.

Primary cilia gradually disappear as G3 MBs develop

In sharp contrast to WNT MB cells, G3 MB cells lacked primary cilia in humans and in a mouse model of G3 MB (Fig. 1). However, precursor cells for G3 MB in a mouse model (Kawauchi et al. 2012)—i.e., *Trp53*$^{-/-}$ GNPs that overexpress MYC—still had primary cilia before being implanted in the brain (Fig. 5A). To determine when cilia disappear from these precursor cells, we implanted G3 MB precursors (*Trp53*$^{-/-}$ GNPs overexpressing MYC) into mouse brains and quantified the cilia in implanted cells at 1, 2, and 3 wk after implantation. Primary cilia gradually shortened and disappeared as the implanted cells expanded and formed tumors (Fig. 5B–D).

Primary cilium loss in G3 MB precursors accelerates tumor development

The gradual cilium loss in implanted G3 MB precursor cells could be a secondary consequence of tumorigenesis. Alternatively, cilium loss may spur tumorigenesis, as it does in *GLI2*-driven MB development (Han et al. 2009). Accordingly, we asked whether cilium loss from G3 MB precursors accelerated tumorigenesis. To remove primary cilia, we transduced *Trp53*$^{-/-}$ GNPs that overexpress MYC with the same shIft88-expressing lentiviruses that we used to remove primary cilia in WNT MB cells. In contrast to WNT MB cells, cilium loss in G3 MB precursors significantly shortened the lives of mice with tumors (Fig. 5E). To understand the cellular mechanism by which cilium loss accelerated tumor growth, we examined cell proliferation and cell death at 3 wk after implantation, when a substantial portion of G3 MB cells still had primary cilia (Fig. 5F) and when mice implanted with shIft88 but not shCTL G3 MB precursors started to succumb to their tumors (Fig. 5E). Cilium loss did not affect cell death (Fig. 5G) but significantly increased BrdU-incorporating cells (Fig. 5H), suggesting that there was increased proliferation. Surprisingly, however, there were fewer cells positive for phospho-histone H3 (PH3), another cell proliferation marker, in shIft88 G3 MBs than in control MBs (Fig. 5I). BrdU labels cells in S phase, whereas PH3 labels cells in late G2 and M phases. The contradictory staining patterns for PH3 and BrdU suggested that cilium loss changed the cell cycle dynamics.

Primary cilium loss in G3 MB precursors aberrantly activates CDK1

To determine whether cilium loss affected cell cycle dynamics, we performed double-thymidine analog analysis and measured the percentage of labeled mitosis (Cai et al. 1997; Hayes and Nowakowski 2000). Three weeks after implanting G3 MB precursors, we injected mice with CldU, IdU, and EdU at 3, 2, and 1 h, respectively, before harvesting their brains (Fig. 6A) and calculated the length of each cell cycle phase (details in the Materials and Methods). Cilium loss shortened the total cell cycle and each phase thereof (Fig. 6A). The G2 phase showed the largest relative decrease in length. The levels of cyclins are tightly regulated during cell cycle progression. Cyclin A accumulates in the nucleus during the S and G2 phases and rapidly declines as cells enter mitosis, whereas cyclin B accumulates in the cytoplasm in G2 and persists until midmitosis (Minshull et al. 1990; Pines and Hunter 1990, 1991). Therefore, cells in G2 strongly express cyclins A and B. To test further whether cilium loss shortened G2, we quantified cells expressing both cyclin A1 and cyclin B2; antibodies against cyclin A2 and cyclin B1 did not stain implanted cells. Cilium loss significantly decreased the proportion of cells expressing both cyclin A1 and cyclin B2 (Fig. 6B,C). Taken together, these results suggested that cilium loss shortened the G2 phase.

To understand the mechanism underlying the shortened G2, we examined the activity of CDK1, a key regulator of G2/M transition. Phosphorylation of tyrosine 15 (pCDK1^{Y15}) by WEE1 and of threonine 14 (pCDK1^{T14}) by MYT1 prevents CDK1 from triggering premature entry into mitosis (Lindqvist et al. 2009). We detected no pCDK1^{T14} by immunostaining in implanted cells, but cilium loss strongly decreased the pCDK1^{Y15} levels (Fig. 6D, E). In controls, most PH3-negative interphase cells, but not PH3-positive mitotic cells, expressed pCDK1^{Y15}, consistent with the low activity of CDK1 in interphase. Remarkably, cilium loss strongly decreased pCDK1^{Y15} in PH3-negative cells, indicating that CDK1 was abnormally activated in interphase cells in the absence of cilia. Of note, CDK1 also plays important roles in S-phase progression (Katsuno et al. 2009). Therefore, abnormal CDK1

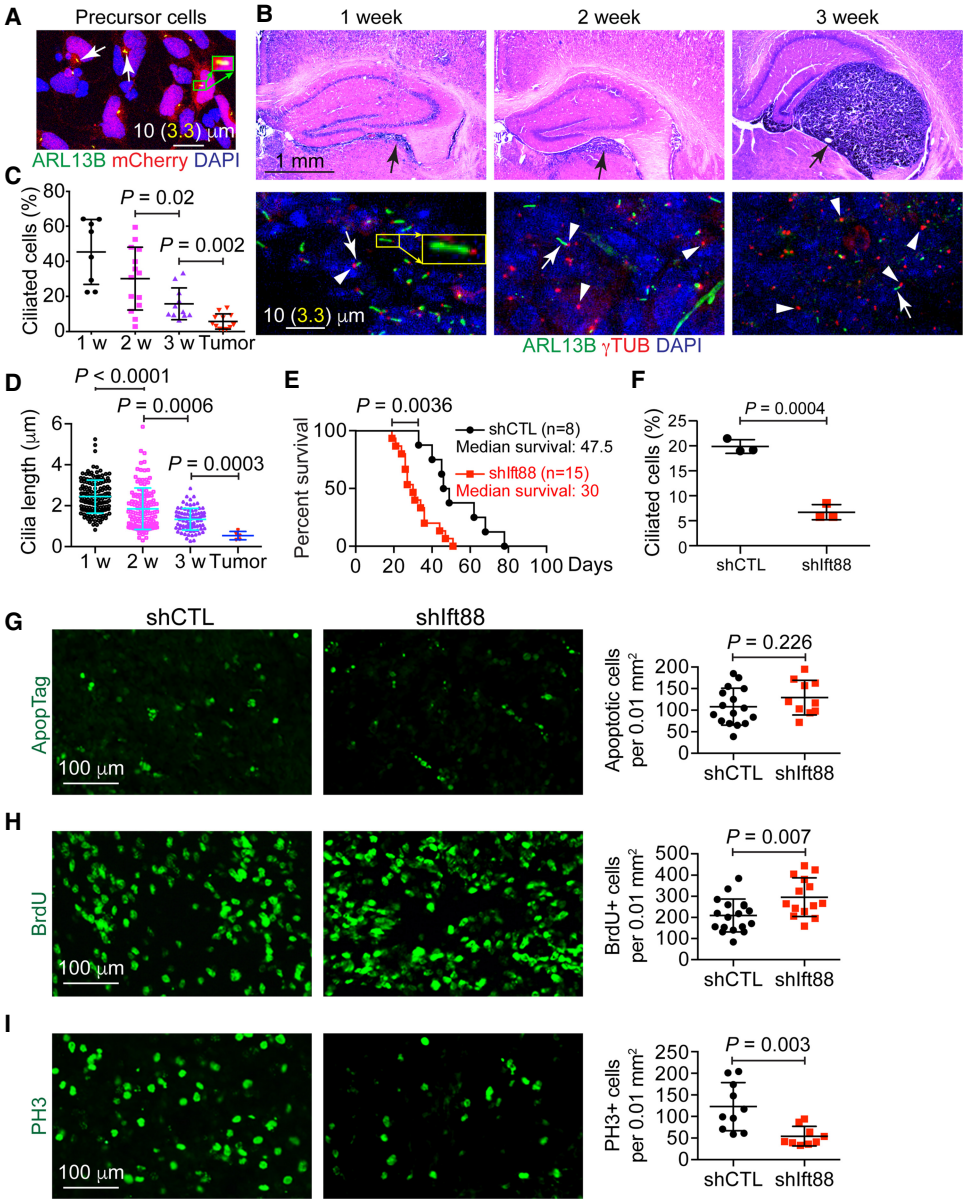

Figure 5. Primary cilium loss promotes G3 MB. (*A*) G3 MB precursors expressing MYC and mCherry (red) had primary cilia (ARL13B, green, arrows) before implantation. (*B–D*) G3 MB precursors gradually lost cilia from 1 to 3 wk after implantation. H&E-stained sections show implanted cells (black arrows). Primary cilia are stained green (ARL13B, white arrows), basal bodies are stained red (γ-tubulin, arrowheads), and nuclei are stained blue (DAPI). Graphs show the mean ± SD (Brown–Forsythe and Welch ANOVA tests with Dunnett's T3 multiple comparison test and Kruskal–Wallis test with Dunn's multiple comparison test for *C* and *D*, respectively). (*E*) Survival curves show that cilium loss (shIft88) in G3 MB precursors shortened survival of tumor-implanted mice (log-rank test). (*F*) Quantification of cilia in G3 MB precursors 3 wk after implantation (mean ± SD, Mann–Whitney test). (*G–I*) Effects of cilium loss (shIft88) on apoptosis (*G*) and proliferation (*H*,*I*) at 3 wk after implantation. Plots show the mean ± SD (unpaired *t*-test). *Insets* are high-magnification images.

activation in the absence of cilia may shorten the S phase and trigger premature G2/M transition.

Cilium loss in G3 MB precursors increases DNA damage and genomic instability

CDK1 activity in middle to late S phase promotes late origin firing in S phase (Katsuno et al. 2009). DNA damage slows down S-phase progression in part by delaying late origin firing, enabling repair of damaged DNA (Ge and Blow 2010; Chao et al. 2017). Accordingly, inhibitory phosphorylation of CDK1 during S phase is important for maintaining genomic integrity (Szmyd et al. 2019). Moreover, G2 is critical for DNA damage repair (O'Connell et al. 2000; Kousholt et al. 2012). Therefore, we asked whether DNA damage was increased in G3 MB precursors lacking cilia. Indeed, cilium loss significantly increased the levels of DNA damage markers pγH2AX^{S139} and pTRIM28^{S824} at

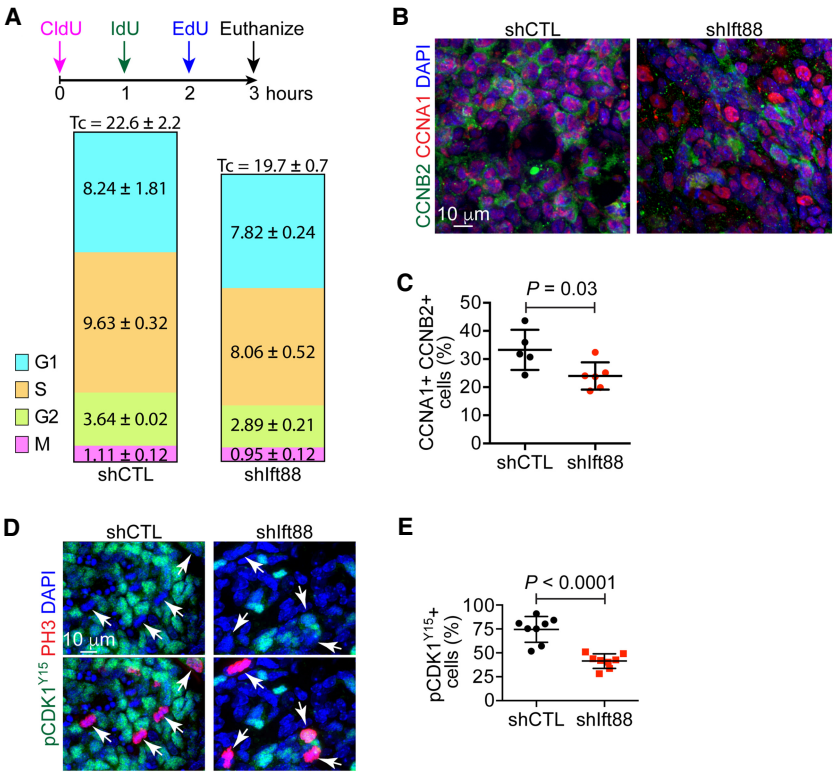

Figure 6. Primary cilium loss shortens the cell cycle and activates CDK1. (*A*) Experimental scheme for labeling proliferating cells by successive injection of different thymidine analogs. Graphs show the length of the cell cycle (Tc) and each cell cycle phase (mean ± SD). (*B*,*C*) Cilium loss decreased cells expressing both CCNA1 (red) and CCNB2 (green). Plots show the mean ± SD (unpaired *t*-test) (*D*,*E*) Cilium loss decreased the proportion of cells expressing pCDK1^{Y15} (green). In controls, most cells except PH3^{+} mitotic cells (red, arrows) express pCDK1^{Y15}. Cilium loss (shIft88) decreased pCDK1^{Y15} in nonmitotic (PH3^{-}) cells. Plots show the mean ± SD (unpaired *t*-test).

3 wk after implantation, as compared with those in control G3 MBs (Fig. 7A,B). Entering mitosis with damaged DNA causes mitotic abnormalities and genomic instability. Fittingly, cilium loss in G3 MB precursors significantly increased mitotic abnormalities, such as chromosome bridges (Fig. 7C) and micronuclei, a well-known indicator of genomic instability (Fig. 7D). Micronuclei increased from 3 wk after implantation to fully transformed tumors in control G3 MBs, and cilium loss accelerated this increase. Together, our findings suggest that cilium loss in G3 MB precursors leads to disrupted cell cycle control and genome instability, characteristics of most cancers and major driving forces for tumorigenesis.

Discussion

Our study has unveiled functions of primary cilia in two fundamental processes that were coaxed to promote tumorigenesis: protein synthesis and cell cycle control. Primary cilia promoted WNT MB growth by facilitating the synthesis of β-catenin, the major oncoprotein driving WNT MB, whereas cilium loss promoted G3 MB growth by abnormally activating CDK1, disrupting cell cycle control, and increasing genome instability. To our knowledge, before this study, activation of SHH signaling was the only known tumor-promoting function of primary cilia and no molecule had been identified as mediating ciliary control of cell cycle progression. We have expanded the repertoire of ciliary functions to include control of protein synthesis and have identified restraining CDK1 activity as a potential mechanism by which cilia control cell cycle progression. These findings provide new frameworks for investigating primary cilium function in normal and pathologic processes, including tumorigenesis.

Extensive genomic and epigenomic profiling has classified MB into four groups and multiple subgroups. Nevertheless, we still need a deep understanding of the tumorigenic mechanisms driving each MB group to develop targeted therapies. WNT MB is characterized and driven by aberrantly stabilized β-catenin, a transcription factor that is rather undruggable. Our finding that cilium-dependent synthesis of β-catenin is important for WNT MB growth revealed an unappreciated and potentially druggable vulnerability in WNT MB. Primary cilia regulated subcellular localization of ELAVL1, an RNA binding protein that shuttles between the nucleus and the cytoplasm. Our findings suggest that nuclear accumulation of ELAVL1 underlies the decreased β-catenin mRNA translation in WNT MB cells lacking cilia. ELAVL1 is overexpressed in many cancers, including MB, and high cytoplasmic ELAVL1 levels correlate with high-grade tumors and poor clinical outcomes (Nabors et al. 2001; Grammatikakis et al. 2017; Schultz et al. 2020). Small molecules targeting ELAVL1 inhibit the growth of several tumors, including ones with high WNT/β-catenin signaling activities (Schultz et al. 2020). Therefore, targeting ELAVL1 to treat WNT MB warrants further preclinical and clinical investigations. Investigating how primary cilia regulate ELAVL1 localization, whether they do so in other cell types, and whether they regulate the translation of mRNAs other than β-catenin mRNA will provide further insights into the role of primary cilia in translation and tumorigenesis.

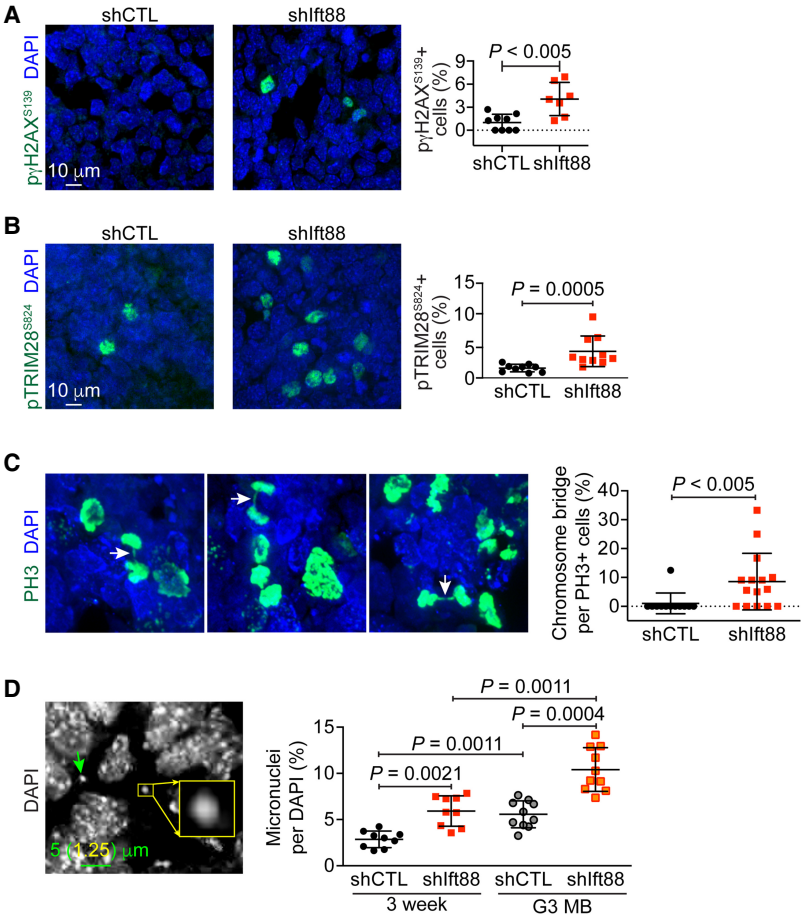

Figure 7. Primary cilium loss increases DNA damage, mitotic defects, and genome instability. (*A*,*B*) Immunofluorescence and quantifications showing that cilium loss (shIft88) increased cells expressing DNA damage markers pγH2AX^{S139} (*A*) and pTRIM28^{S824} (*B*). Plots show the mean ± SD (Mann–Whitney test). (*C*) Examples of mitotic defects (chromosome bridge, arrows) in mitotic shIft88 WNT MB cells (PH3^{+}, green). Plots show the mean ± SD (Mann–Whitney test). (*D*) Cilium loss (shIft88) increased micronuclei (arrows). Nuclei were stained with DAPI. The *inset* is a high-magnification image. Plots show the mean ± SD (Brown–Forsythe and Welch ANOVA tests with Dunnet's T3 multiple comparison test).

Cilium loss increased granules containing β-catenin mRNA and G3BP1, a canonical marker of stress granules, consistent with the decreased translation of β-catenin mRNA. Stress granules are membraneless organelles consisting of ribonucleoproteins that form from mRNAs stalled in translation initiation to cope with various cellular stresses (Kedersha et al. 2013; Protter and Parker 2016). Reduced cytoplasmic ELAVL1 in the absence of cilia might facilitate stress granule formation by increasing "naked mRNAs"; cytoplasmic ELAVL1 inversely correlates with the level of stress granules (Bounedjah et al. 2014). Stress granules are thought to function as sorting and storage sites for mRNAs during stress-induced translation repression. Although stress granules do not affect overall translation, several studies have pointed to their role in mRNA sequestration in translation inhibition (Sahoo et al. 2018; Simon et al. 2019; Tsang et al. 2019). Stress granule formation might further repress translation of β-catenin mRNA by sequestering it or might be a consequence of decreased translation. Notably, stress granules enable certain cancer cells to progress and to resist chemotherapeutic agents (Fournier et al. 2010; Kaehler et al. 2014; Adjibade et al. 2015; Anderson et al. 2015; Somasekharan et al. 2015; Grabocka and Bar-Sagi 2016). Although cilium loss strongly impeded WNT MB growth, the tumors eventually grew in some mice, which displayed abundant G3BP1-positive granules; therefore, stress granules may confer resistance to the inhibitory effects of cilium loss, helping MB to grow rather than inhibiting β-catenin mRNA translation.

It has long been speculated that primary cilia function as a structural checkpoint for G2/M-phase transition in proliferating cells because they must be disassembled to release the basal body before the M phase; however, this has not been shown experimentally. Moreover, although several studies have demonstrated mechanisms by which cell cycle regulators control cilium assembly and disassembly (Izawa et al. 2015; Wang and Dynlacht 2018), studies showing that primary cilia control the cell cycle have been largely observational and have not elaborated on the regulatory mechanisms (Bielas et al. 2009; Jacoby et al. 2009; Kim et al. 2011; Li et al. 2011; Inoko et al. 2012; Yang et al. 2013; Gabriel et al. 2016). Here we have shown that, in G3 MB precursor cells, cilium loss shortened the cell cycle and the G2 phase and that aberrant CDK1 activation may underlie the premature G2/M transition. Therefore, primary cilia function not only as a passive structural barrier for G2/M transition but also as an active negative regulator of a key driver of G2/M transition. Primary cilium loss also increased DNA damage and genome instability, enabling the accumulation of genetic alterations required for the evolution of cancerous cells. Notably, genomic instability is characteristic of G3 MB and has been proposed as an early

driver in a large proportion of G3 MBs (Jones et al. 2012; Northcott et al. 2012, 2017; Pugh et al. 2012). Moreover, inhibitors of the cell cycle machinery have emerged as a common theme among small molecules inhibiting G3 MB (Endersby et al. 2021). Our data showing that disrupted cell cycle control and genome instability driven by cilium loss promote G3 MB suggest a mechanism for the phenomena observed in genomics and drug screening. Beyond G3 MB, most human tumors lack primary cilia, and the frequency of cilia decreases in some tumors as they progress (Eguether and Hahne 2018; Liu et al. 2018). Cilium loss may contribute to the development and progress of these tumors by disrupting cell cycle control and increasing genome instability.

Dysregulated translation and cell cycle control are hallmarks of and major driving forces in tumorigenesis. Further studies of the mechanisms by which primary cilia regulate translation and the cell cycle and of whether such mechanisms control the development of diverse tumor types will advance our understanding of tumorigenic mechanisms and the function of primary cilia.

Materials and methods

Human medulloblastoma samples

Four-micrometer formalin-fixed and paraffin-embedded tissue sections were collected from selected diagnostic tumor samples on clinical trial SJMB03 (ClinicalTrials.gov identifier NCT00085202). Molecular subtyping was performed using immunohistochemistry and DNA methylation profiling as described previously (Gajjar et al. 2021).

Mice

Animal procedures were approved by the Institutional Animal Care and Use Committee of St. Jude Children's Research Hospital. The primary WNT MB mouse model [*Blbp::Cre; Ctnnb*$^{loxp(ex3)/+}$*; Pik3ca*$^{loxp(E545K)/+}$] was described previously (Robinson et al. 2012). For the secondary WNT MB model, we dissociated the primary WNT MBs with Accutase (Stem Cell Technologies 07920) for 15 min at 37°C and grew dissociated MB cells in neurobasal medium (Gibco 21103049) containing 1× N-2 supplement (Gibco 17502-048), 1× B-27 supplement (Gibco 17504-044), 10 ng/mL human bFGF (PeproTech AF-100-18B), and 10 ng/mL human EGF (PeproTech AF-100-15). We transduced WNT MB cells with shCTL or shIft88 lentivirus that also expressed mCherry. We isolated transduced WNT MB cells by FACS and implanted 1×10^6 WNT MB cells suspended in Matrigel (Corning 356234) in the cerebella of 2-mo-old CD-1 nu/nu mice (Charles River) through the cisterna magna.

The mouse model of G3 MB was described previously (Kawauchi et al. 2012). We dissociated P6 or P7 *Trp53*$^{-/-}$ mouse cerebella with Accutase for 15 min at 37°C. We loaded cells on a 35% and 60% Percoll gradient and centrifuged at 2000*g* for 15 min to purify GNPs. Purified GNPs were seeded at 1×10^6 cells/well in six-well plates coated with poly-D-lysin and Matrigel and grown in neurobasal medium containing 1× antibiotic–antimycotic solution (Thermo Scientific 15240062), 1× GlutaMAX (Gibco 35050-061), 0.5% glucose (Sigma-Aldrich G8769), 1× SPITE (Sigma-Aldrich S5666), 1× oleic acid albumin/linoleic acid (Sigma-Aldrich L9655), 1× B-27, 1× N-2, 1.5 µg/mL N-acetyl-L-cysteine (Sigma A9165), and 15% SHH-conditioned neurobasal medium. After 1 h in culture, we transduced cells with retroviruses expressing both MYC and GFP. The next day, we transduced cells with shCTL or shIft88 lentiviruses that also expressed mCherry. The medium was changed 48 h after the last lentivirus treatment, and the cells were maintained in culture for 2 d. Transduced GNPs were then isolated by FACS and implanted in the cortices of 2-mo-old CD-1 nu/nu mice.

Virus production

Lentivirus was produced in HEK293T cells (ATCC CRL-3216) by cotransfecting helper vectors (6 µg of pCAG-VSVG, 2 µg of pCAG-KGP1-RPE, and 2 µg of pCAG-RTR2) and 12 µg of shRNA vectors (transOMIC Technologies) with Lipofectamine 3000 (Invitrogen). After overnight transfection, the medium was replaced with Dulbecco's modified Eagle's medium (DMEM) containing 10% FBS. At 24 h after transfection, the medium was replaced with collection medium (neurobasal medium containing 1× N-2, 1× B-27, and 1× antibiotic-antimycotic solution). The retroviruses expressing MYC and GFP (or mCherry) were produced as described previously (Kawauchi et al. 2012).

WNT MB cell culture

We grew WNT MB cells in six-well plates coated with poly-D-lysine and Matrigel. When the cells were ~80% confluent, we treated them with 50 µM cycloheximide (Sigma-Aldrich 01810) for 16 h and then replaced the medium with fresh medium containing 10 µM MG132 (Millipore M8699) and no cycloheximide. Cells were harvested before the medium was changed and at 2, 4, 6, and 8 h thereafter.

Bioluminescence imaging

Three weeks after implanting WNT MB cells, we injected mice intraperitoneally with a 30 mg/mL solution of D-luciferin (Promega) in PBS at 150 mg/kg. After injection, animals were anesthetized using isoflurane and maintained via a nosecone on a heated imaging bed within the system during the scan. Optical imaging was performed using an IVIS Spectrum or IVIS-200 imaging system (PerkinElmer).

Western blot analysis

We lysed cells in RIPA buffer (50 mM Tris-HCl at pH 8.0, 150 mM NaCl, 1% Nonidet P-40, 0.5% sodium deoxycholate, 0.1% SDS) containing protease inhibitor cocktail (Millipore 524627). Protein samples were denatured and reduced with Laemmli buffer (Bio-Rad 161-0634), separated on a NuPAGE 4%–12% Bis-Tris gel (Invitrogen NP0323), and transferred to a PVDF membrane (Millipore IPVH00010). The PVDF membrane was incubated with blocking buffer (5% skim milk in TBST buffer) for 1 h at room temperature, rinsed in TBST buffer (20 mM Tris-Cl, 150 mM NaCl, 0.1% Tween20 at pH 7.6), incubated with primary antibody overnight at 4°C, washed in TBST, and incubated with HRP-conjugated secondary antibody (diluted 1:10,000–1:20,000) for 1–2 h at room temperature. The protein band was detected with SuperSignal West Dura extended duration substrate (Thermo Scientific 34076).

Immunostaining

We perfused mice with 4% paraformaldehyde (PFA; Electron Microscopic Science 15714-S). Their brains were further fixed overnight in 4% PFA at 4°C, washed in PBS, cryoprotected in 30%

sucrose, embedded in OCT (Tissue-Tek 4583), and sectioned at a thickness of 12 µm. Cells grown in culture were fixed with 4% PFA for 15 min at 4°C and then washed with PBS. Sections were subjected to an antigen-unmasking step in citrate buffer (pH 6.0) using a rice cooker (Oster) for 15 min with hot steam and incubated for 1 h in blocking buffer (5% normal donkey serum [Sigma-Aldrich A4503], 0.05% Triton X-100 [Sigma-Aldrich T8787] in PBS). Sections were incubated with primary antibodies in blocking buffer overnight at 4°C, washed in PBS, incubated with secondary antibodies in blocking buffer for 1 h at room temperature, washed in PBS, incubated with DAPI (Cayman Chemical 14285), washed in PBS, and mounted with fluorescent mounting medium (PolyScience 18606-20). We used the following antibodies: acetylated tubulin (1:200; Sigma-Aldrich T7451), γ-tubulin (1:1000; Sigma-Aldrich T5192), ARL13B (1:2000; University of California at Davis NeuroMap), pericentrin (1:1000; Abcam ab4448), β-catenin (1:100; BD Transduction Laboratories 610514), ELAVL1 (1:400; Abcam ab200342, and 1:400; Abcam ab28660), phospho-histone 3 (1:500; Cell Signaling Technology 9706), BrdU (1:150; Abcam 1893), CldU (1:100; Novus Biologicals NB500-169), IdU (1:100; BD Biosciences 347580), Ki67 (1:500; Abcam ab15580), TUJ1 (1:100; Covance MMS-435P), phospho-CDK1 (Tyr15; 1:100; Cell Signaling Technology 1144451), phospho-histone H2A.X (1:400; Cell Signaling Technology 2577S), phospho-TRIM28 (1:100; Bethyl Laboratories A300-767A), and G3BP1 (1:400; BD Biosciences 611147). We used Alexa fluor-conjugated secondary antibodies (1:500; Thermo Fisher Scientific or Jackson ImmunoResearch).

In situ hybridization

We purchased custom LNA mRNA detection probes for *Ctnnb1* (Exiqon 300500, design IDs 703075 and 676113-1). Tissue sections were digested with 20 µg/mL proteinase K in prewarmed 50 mM Tris for 10–20 min at 37°C; rinsed three times in distilled water; immersed in ice-cold 20% (v/v) acetic acid for 20 sec; dehydrated sequentially in 70%, 95%, and 100% ethanol for 1 min each; air-dried; and prehybridized with 100 µL of hybridization solution (50% deionized formamide, 0.2× SSC buffer, 50 mM sodium phosphate at pH 7.0, 10% dextran sulfate) for 1 h in a humidified hybridization chamber at 62°C. Prehybridized sections were incubated with hybridization solution containing 50–100 µL of probe in the humidified hybridization chamber for 2 h at 65°C, washed three times with 50% formamide in 2× SSC for 5 min at 65°C, washed three times with 0.1× SSC for 5 min at room temperature, and incubated with FITC-conjugated Avidin (Vector Laboratories A2001). Subsequently, DNA was stained with DAPI and sections were mounted with fluorescent mounting medium (PolyScience 18606-20). For combined in situ hybridization and immunofluorescence studies, *Ctnnb1* in situ hybridization was performed as described above except that the temperature for hybridization was 42°C. The sections were then immunostained for G3BP1 as described above.

H&E staining

Sections were rinsed in PBS, incubated in hematoxylin solution (Sigma-Aldrich HHS-32) for 6 min, rinsed in tap water for 20 min, decolorized in 0.25% acid alcohol for 1–2 sec, rinsed in tap water for 5 min, counterstained with eosin (Thermo Scientific 7111) for 15 sec, dehydrated sequentially in 95% and 100% ethanol for 3 min each, cleared in xylene solution, and mounted with Cytoseal (Thermo Scientific 8312-4).

TUNEL assay

The ApopTag Plus in situ apoptosis fluorescein detection kit (Millipore Sigma S7111) was used following the manufacturer's protocol.

Cell cycle kinetics

Mice were injected with CldU at 3 h, IdU at 2 h, and EdU at 1 h before euthanasia. The cells that had left S phase during the 1-h interval between the IdU and EdU injections were marked as IdU^+EdU^- (L cells = IdU^+EdU^-). The ratio of the length of one cell cycle period to that of another period is equal to the ratio of the number of cells in each of those periods. Thus, the length of the S phase (T_S) was determined from the equation 1 h/Ts = L cells/S cells, where S cells were EdU^+ cells, and the length of the cell cycle (T_C) was determined from T_S/T_C = S cells/($Ki67^+$ proliferating cells). To determine the length of the M phase (T_M), M-phase cells were identified as $PH3^+$ cells with mitotic shape. The proportion of mitotic cells (M fraction = mitotic cells/$Ki67^+$ proliferating cells) was used to calculate T_M, where T_M = M fraction/T_C. The time required for all mitotic cells to be positive for thymidine analogs (CldU, IdU, or EdU) was equal to T_{G2+M}. To calculate T_{G2+M}, the mitotic labeling index (MLI; the percentage of thymidine analog-labeled mitotic cells out of the total mitotic cells) was determined and then plotted as a function of time. From this plot, T_{G2+M} was calculated when the MLI would be 100%. T_{G1} was calculated from $T_{G1} = T_C - (T_S + T_{G2+M})$, and T_{G2} was calculated from $T_{G2} = T_{G2+M} - T_m$.

RNA sequencing and RT-qPCR

RNA was extracted from tumors with an RNeasy mini kit (Qiagen). A sequencing library was prepared using a TruSeq stranded total RNA kit (Illumina) and sequenced with an Illumina HiSeq system. FastQ sequences were mapped to the mm9 genome and counted with HTSEQ54, and the gene-level fragments per kilobase of transcript per million values were then computed. We used Ingenuity Pathway Analysis (Qiagen) to analyze RNA-seq data. For RT-qPCR, cDNA was synthesized using SuperScript III reverse transcriptase. qPCR was performed with Power SYBR Green PCR master mix (Applied Biosystems). Transcript levels were normalized to those of *Gapdh*. Supplemental Table S1 shows primers for qPCR. The RNA sequencing data have been deposited in Gene Expression Omnibus (GSE207008).

Statistical analysis

We used GraphPad Prism for statistical analysis. All statistical analyses were two tailed. Data were pretested for normality by the D'Agostino–Pearson test. We used an unpaired *t*-test and the Mann–Whitney test for normal distribution data and for nonparametric analysis, respectively. For multiple comparisons, we used ANOVA and Kruskal–Wallis tests for normal distribution data and for nonparametric analysis, respectively. We used a log-rank test for the survival analysis. *P*-values of <0.05 were considered to indicate significance.

Competing interest statement

The authors declare no competing interests.

Acknowledgments

We thank L.S. Goldstein at the University of California at San Diego for the *Kif3a*$^{fl/fl}$ mice, and J. Houston and K. Lowe for help with FACS. We thank the staff of the Animal Resource Center, the Hartwell Center for Bioinformatics and Biotechnology, the Center for In Vivo Imaging and Therapeutics, and the Cell and Tissue Imaging Center at St. Jude Children's Research Hospital for technical assistance. We thank T. Mori and X. Cao for help with statistical analyses and for reviewing the manuscript, respectively. We thank Keith A. Laycock, PhD, ELS, for scientific editing of the manuscript. This work was supported by National Institutes of Health/National Cancer Institute Cancer Center Core Support grant CA021765 (to St. Jude Children's Research Hospital), the Sontag Foundation Distinguished Scientist Award (to Y.-G.H.), CA096832 (to M.F.R.), and American Lebanese Syrian Associated Charities. The content of this manuscript is solely the responsibility of the authors and does not necessarily represent the official views of the National Institutes of Health.

Author contributions: Y.H.Y. performed experiments with help from S.H. and C.-C.W. D.K. performed the time-course experiments for G3 MB. B.A.O. and G.W.R. provided human MB samples. D.F. analyzed RNA-seq data. M.M.T. provided *Ctnnb1*$^{loxP(ex3)}$ mice. R.J.G. and M.F.R. helped generate WNT and G3 MB mouse models. Y.H.Y. and Y.-G.H. wrote the manuscript. Y.-G.H. supervised the project.

References

Adjibade P, Grenier St-Sauveur V, Quevillon Huberdeau M, Fournier M-J, Savard A, Coudert L, Khandjian EW, Mazroui R. 2015. Sorafenib, a multikinase inhibitor, induces formation of stress granules in hepatocarcinoma cells. *Oncotarget* **6:** 43927–43943. doi:10.18632/oncotarget.5980

Anderson P, Kedersha N, Ivanov P. 2015. Stress granules, P-bodies and cancer. *Biochim Biophys Acta* **1849:** 861–870. doi:10.1016/j.bbagrm.2014.11.009

Atasoy U, Watson J, Patel D, Keene JD. 1998. ELAV protein HuA (HuR) can redistribute between nucleus and cytoplasm and is upregulated during serum stimulation and T cell activation. *J Cell Sci* **111:** 3145–3156. doi:10.1242/jcs.111.21.3145

Bielas SL, Silhavy JL, Brancati F, Kisseleva MV, Al-Gazali L, Sztriha L, Bayoumi RA, Zaki MS, Abdel-Aleem A, Rosti RO, et al. 2009. Mutations in *INPP5E*, encoding inositol polyphosphate-5-phosphatase E, link phosphatidyl inositol signaling to the ciliopathies. *Nat Genet* **41:** 1032–1036. doi:10.1038/ng.423

Bounedjah O, Desforges B, Wu T-D, Pioche-Durieu C, Marco S, Hamon L, Curmi PA, Guerquin-Kern J-L, Piétrement O, Pastré D. 2014. Free mRNA in excess upon polysome dissociation is a scaffold for protein multimerization to form stress granules. *Nucleic Acids Res* **42:** 8678–8691. doi:10.1093/nar/gku582

Cai L, Hayes NL, Nowakowski RS. 1997. Local homogeneity of cell cycle length in developing mouse cortex. *J Neurosci* **17:** 2079–2087. doi:10.1523/JNEUROSCI.17-06-02079.1997

Cao C, Sun J, Zhang D, Guo X, Xie L, Li X, Wu D, Liu L. 2015. The long intergenic noncoding RNA UFC1, a target of microRNA 34a, interacts with the mRNA stabilizing protein HuR to increase levels of β-catenin in HCC cells. *Gastroenterology* **148:** 415–426.e18. doi:10.1053/j.gastro.2014.10.012

Chao HX, Poovey CE, Privette AA, Grant GD, Chao HY, Cook JG, Purvis JE. 2017. Orchestration of DNA damage checkpoint dynamics across the human cell cycle. *Cell Syst* **5:** 445–459.e5. doi:10.1016/j.cels.2017.09.015

Chou S-D, Murshid A, Eguchi T, Gong J, Calderwood SK. 2015. HSF1 regulation of β-catenin in mammary cancer cells through control of HuR/elavL1 expression. *Oncogene* **34:** 2178–2188. doi:10.1038/onc.2014.177

Eguether T, Hahne M. 2018. Mixed signals from the cell's antennae: primary cilia in cancer. *EMBO Rep* **19:** e46589. doi:10.15252/embr.201846589

Endersby R, Whitehouse J, Pribnow A, Kuchibhotla M, Hii H, Carline B, Gande S, Stripay J, Ancliffe M, Howlett M, et al. 2021. Small-molecule screen reveals synergy of cell cycle checkpoint kinase inhibitors with DNA-damaging chemotherapies in medulloblastoma. *Sci Transl Med* **13:** eaba7401. doi:10.1126/scitranslmed.aba7401

Fan XC, Steitz JA. 1998. Overexpression of HuR, a nuclear-cytoplasmic shuttling protein, increases the in vivo stability of ARE-containing mRNAs. *EMBO J* **17:** 3448–3460. doi:10.1093/emboj/17.12.3448

Fournier M-J, Gareau C, Mazroui R. 2010. The chemotherapeutic agent bortezomib induces the formation of stress granules. *Cancer Cell Int* **10:** 12. doi:10.1186/1475-2867-10-12

Gabriel E, Wason A, Ramani A, Gooi LM, Keller P, Pozniakovsky A, Poser I, Noack F, Telugu NS, Calegari F, et al. 2016. CPAP promotes timely cilium disassembly to maintain neural progenitor pool. *EMBO J* **35:** 803–819. doi:10.15252/embj.201593679

Gajjar A, Robinson GW, Smith KS, Lin T, Merchant TE, Chintagumpala M, Mahajan A, Su J, Bouffet E, Bartels U, et al. 2021. Outcomes by clinical and molecular features in children with medulloblastoma treated with risk-adapted therapy: results of an international phase III trial (SJMB03). *J Clin Oncol* **39:** 822–835. doi:10.1200/JCO.20.01372

Ge XQ, Blow JJ. 2010. Chk1 inhibits replication factory activation but allows dormant origin firing in existing factories. *J Cell Biol* **191:** 1285–1297. doi:10.1083/jcb.201007074

Gibson P, Tong Y, Robinson G, Thompson MC, Currle DS, Eden C, Kranenburg TA, Hogg T, Poppleton H, Martin J, et al. 2010. Subtypes of medulloblastoma have distinct developmental origins. *Nature* **468:** 1095–1099. doi:10.1038/nature09587

Grabocka E, Bar-Sagi D. 2016. Mutant KRAS enhances tumor cell fitness by upregulating stress granules. *Cell* **167:** 1803–1813.e12. doi:10.1016/j.cell.2016.11.035

Grammatikakis I, Abdelmohsen K, Gorospe M. 2017. Posttranslational control of HuR function. *Wiley Interdiscip Rev RNA* **8:** e1372. doi:10.1002/wrna.1372

Han YG, Kim HJ, Dlugosz AA, Ellison DW, Gilbertson RJ, Alvarez-Buylla A. 2009. Dual and opposing roles of primary cilia in medulloblastoma development. *Nat Med* **15:** 1062–1065. doi:10.1038/nm.2020

Harada N, Tamai Y, Ishikawa T, Sauer B, Takaku K, Oshima M, Taketo MM. 1999. Intestinal polyposis in mice with a dominant stable mutation of the β-catenin gene. *EMBO J* **18:** 5931–5942. doi:10.1093/emboj/18.21.5931

Hayes NL, Nowakowski RS. 2000. Exploiting the dynamics of S-phase tracers in developing brain: interkinetic nuclear migration for cells entering versus leaving the S-phase. *Dev Neurosci* **22:** 44–55. doi:10.1159/000017426

Inoko A, Matsuyama M, Goto H, Ohmuro-Matsuyama Y, Hayashi Y, Enomoto M, Ibi M, Urano T, Yonemura S, Kiyono T, et al. 2012. Trichoplein and Aurora A block aberrant primary cilia assembly in proliferating cells. *J Cell Biol* **197:** 391–405. doi:10.1083/jcb.201106101

Izawa I, Goto H, Kasahara K, Inagaki M. 2015. Current topics of functional links between primary cilia and cell cycle. *Cilia* **4:** 12. doi:10.1186/s13630-015-0021-1

Jacoby M, Cox JJ, Gayral S, Hampshire DJ, Ayub M, Blockmans M, Pernot E, Kisseleva MV, Compère P, Schiffmann SN, et al. 2009. *INPP5E* mutations cause primary cilium signaling defects, ciliary instability and ciliopathies in human and mouse. *Nat Genet* **41:** 1027–1031. doi:10.1038/ng.427

Jenks AD, Vyse S, Wong JP, Kostaras E, Keller D, Burgoyne T, Shoemark A, Tsalikis A, de la Roche M, Michaelis M, et al. 2018. Primary cilia mediate diverse kinase inhibitor resistance mechanisms in cancer. *Cell Rep* **23:** 3042–3055. doi:10.1016/j.celrep.2018.05.016

Jones DT, Jäger N, Kool M, Zichner T, Hutter B, Sultan M, Cho Y-J, Pugh TJ, Hovestadt V, Stütz AM, et al. 2012. Dissecting the genomic complexity underlying medulloblastoma. *Nature* **488:** 100–105. doi:10.1038/nature11284

Juraschka K, Taylor MD. 2019. Medulloblastoma in the age of molecular subgroups: a review. *J Neurosurg Pediatr* **24:** 353–363. doi:10.3171/2019.5.PEDS18381

Kaehler C, Isensee J, Hucho T, Lehrach H, Krobitsch S. 2014. 5-fluorouracil affects assembly of stress granules based on RNA incorporation. *Nucleic Acids Res* **42:** 6436–6447. doi:10.1093/nar/gku264

Katsuno Y, Suzuki A, Sugimura K, Okumura K, Zineldeen DH, Shimada M, Niida H, Mizuno T, Hanaoka F, Nakanishi M. 2009. Cyclin A–Cdk1 regulates the origin firing program in mammalian cells. *Proc Natl Acad Sci* **106:** 3184–3189. doi:10.1073/pnas.0809350106

Kawauchi D, Robinson G, Uziel T, Gibson P, Rehg J, Gao C, Finkelstein D, Qu C, Pounds S, Ellison DW, et al. 2012. A mouse model of the most aggressive subgroup of human medulloblastoma. *Cancer Cell* **21:** 168–180. doi:10.1016/j.ccr.2011.12.023

Kedersha N, Ivanov P, Anderson P. 2013. Stress granules and cell signaling: more than just a passing phase? *Trends Biochem Sci* **38:** 494–506. doi:10.1016/j.tibs.2013.07.004

Kim S, Zaghloul NA, Bubenshchikova E, Oh EC, Rankin S, Katsanis N, Obara T, Tsiokas L. 2011. Nde1-mediated inhibition of ciliogenesis affects cell cycle re-entry. *Nat Cell Biol* **13:** 351–360. doi:10.1038/ncb2183

Kousholt AN, Menzel T, Storgaard Sørensen C. 2012. Pathways for genome integrity in G2 phase of the cell cycle. *Biomolecules* **2:** 579–607. doi:10.3390/biom2040579

Li A, Saito M, Chuang J-Z, Tseng Y-Y, Dedesma C, Tomizawa K, Kaitsuka T, Sung C-H. 2011. Ciliary transition zone activation of phosphorylated Tctex-1 controls ciliary resorption, S-phase entry and fate of neural progenitors. *Nat Cell Biol* **13:** 402–411. doi:10.1038/ncb2218

Lindqvist A, Rodríguez-Bravo V, Medema RH. 2009. The decision to enter mitosis: feedback and redundancy in the mitotic entry network. *J Cell Biol* **185:** 193–202. doi:10.1083/jcb.200812045

Liu H, Kiseleva AA, Golemis EA. 2018. Ciliary signalling in cancer. *Nat Rev Cancer* **18:** 511–524. doi:10.1038/s41568-018-0023-6

López de Silanes I, Fan J, Yang X, Zonderman AB, Potapova O, Pizer ES, Gorospe M. 2003. Role of the RNA-binding protein HuR in colon carcinogenesis. *Oncogene* **22:** 7146–7154. doi:10.1038/sj.onc.1206862

Marszalek JR, Ruiz-Lozano P, Roberts E, Chien KR, Goldstein LS. 1999. Situs inversus and embryonic ciliary morphogenesis defects in mouse mutants lacking the KIF3A subunit of kinesin-II. *Proc Natl Acad Sci* **96:** 5043–5048. doi:10.1073/pnas.96.9.5043

Marszalek JR, Liu X, Roberts EA, Chui D, Marth JD, Williams DS, Goldstein LS. 2000. Genetic evidence for selective transport of opsin and arrestin by kinesin-II in mammalian photoreceptors. *Cell* **102:** 175–187. doi:10.1016/S0092-8674(00)00023-4

Minshull J, Golsteyn R, Hill CS, Hunt T. 1990. The A- and B-type cyclin associated cdc2 kinases in *Xenopus* turn on and off at different times in the cell cycle. *EMBO J* **9:** 2865–2875. doi:10.1002/j.1460-2075.1990.tb07476.x

Mukhopadhyay S, Wen X, Chih B, Nelson CD, Lane WS, Scales SJ, Jackson PK. 2010. TULP3 bridges the IFT-A complex and membrane phosphoinositides to promote trafficking of G protein-coupled receptors into primary cilia. *Genes Dev* **24:** 2180–2193. doi:10.1101/gad.1966210

Nabors LB, Gillespie GY, Harkins L, King PH. 2001. Hur, a RNA stability factor, is expressed in malignant brain tumors and binds to adenine- and uridine-rich elements within the 3′ untranslated regions of cytokine and angiogenic factor mRNAs. *Cancer Res* **61:** 2154–2161.

Northcott PA, Shih DJ, Peacock J, Garzia L, Morrissy AS, Zichner T, Stütz AM, Korshunov A, Reimand J, Schumacher SE, et al. 2012. Subgroup-specific structural variation across 1,000 medulloblastoma genomes. *Nature* **488:** 49–56. doi:10.1038/nature11327

Northcott PA, Buchhalter I, Morrissy AS, Hovestadt V, Weischenfeldt J, Ehrenberger T, Gröbner S, Segura-Wang M, Zichner T, Rudneva VA, et al. 2017. The whole-genome landscape of medulloblastoma subtypes. *Nature* **547:** 311–317. doi:10.1038/nature22973

Northcott PA, Robinson GW, Kratz CP, Mabbott DJ, Pomeroy SL, Clifford SC, Rutkowski S, Ellison DW, Malkin D, Taylor MD, et al. 2019. Medulloblastoma. *Nat Rev Dis Primers* **5:** 11. doi:10.1038/s41572-019-0063-6

O'Connell MJ, Walworth NC, Carr AM. 2000. The G2-phase DNA-damage checkpoint. *Trends Cell Biol* **10:** 296–303. doi:10.1016/S0962-8924(00)01773-6

Palomo-Irigoyen M, Pérez-Andrés E, Iruarrizaga-Lejarreta M, Barreira-Manrique A, Tamayo-Caro M, Vila-Vecilla L, Moreno-Cugnon L, Beitia N, Medrano D, Fernández-Ramos D, et al. 2020. Hur/ELAVL1 drives malignant peripheral nerve sheath tumor growth and metastasis. *J Clin Invest* **130:** 3848–3864. doi:10.1172/JCI130379

Pazour GJ, Dickert BL, Vucica Y, Seeley ES, Rosenbaum JL, Witman GB, Cole DG. 2000. *Chlamydomonas* IFT88 and its mouse homologue, polycystic kidney disease gene *Tg*737, are required for assembly of cilia and flagella. *J Cell Biol* **151:** 709–718. doi:10.1083/jcb.151.3.709

Peng SS, Chen CY, Xu N, Shyu AB. 1998. RNA stabilization by the AU-rich element binding protein, HuR, an ELAV protein. *EMBO J* **17:** 3461–3470. doi:10.1093/emboj/17.12.3461

Pines J, Hunter T. 1990. Human cyclin A is adenovirus E1A-associated protein p60 and behaves differently from cyclin B. *Nature* **346:** 760–763. doi:10.1038/346760a0

Pines J, Hunter T. 1991. Human cyclins A and B1 are differentially located in the cell and undergo cell cycle-dependent nuclear transport. *J Cell Biol* **115:** 1–17. doi:10.1083/jcb.115.1.1

Protter DSW, Parker R. 2016. Principles and properties of stress granules. *Trends Cell Biol* **26:** 668–679. doi:10.1016/j.tcb.2016.05.004

Pugh TJ, Weeraratne SD, Archer TC, Pomeranz Krummel DA, Auclair D, Bochicchio J, Carneiro MO, Carter SL, Cibulskis K, Erlich RL, et al. 2012. Medulloblastoma exome sequencing uncovers subtype-specific somatic mutations. *Nature* **488:** 106–110. doi:10.1038/nature11329

Qin J, Lin Y, Norman RX, Ko HW, Eggenschwiler JT. 2011. Intraflagellar transport protein 122 antagonizes Sonic Hedgehog

signaling and controls ciliary localization of pathway components. *Proc Natl Acad Sci* **108:** 1456–1461. doi:10.1073/pnas.1011410108

Robinson G, Parker M, Kranenburg TA, Lu C, Chen X, Ding L, Phoenix TN, Hedlund E, Wei L, Zhu X, et al. 2012. Novel mutations target distinct subgroups of medulloblastoma. *Nature* **488:** 43–48. doi:10.1038/nature11213

Rosenbaum JL, Witman GB. 2002. Intraflagellar transport. *Nat Rev Mol Cell Biol* **3:** 813–825. doi:10.1038/nrm952

Sahoo PK, Lee SJ, Jaiswal PB, Alber S, Kar AN, Miller-Randolph S, Taylor EE, Smith T, Singh B, Ho TS-Y, et al. 2018. Axonal G3BP1 stress granule protein limits axonal mRNA translation and nerve regeneration. *Nat Commun* **9:** 3358. doi:10.1038/s41467-018-05647-x

Schultz CW, Preet R, Dhir T, Dixon DA, Brody JR. 2020. Understanding and targeting the disease-related RNA binding protein human antigen R (HuR). *Wiley Interdiscip Rev RNA* **11:** e1581. doi:10.1002/wrna.1581

Simon JR, Eghtesadi SA, Dzuricky M, You L, Chilkoti A. 2019. Engineered ribonucleoprotein granules inhibit translation in protocells. *Mol Cell* **75:** 66–75.e5. doi:10.1016/j.molcel.2019.05.010

Somasekharan SP, El-Naggar A, Leprivier G, Cheng H, Hajee S, Grunewald TGP, Zhang F, Ng T, Delattre O, Evdokimova V, et al. 2015. YB-1 regulates stress granule formation and tumor progression by translationally activating G3BP1. *J Cell Biol* **208:** 913–929. doi:10.1083/jcb.201411047

Stottmann RW, Tran PV, Turbe-Doan A, Beier DR. 2009. *Ttc21b* is required to restrict sonic hedgehog activity in the developing mouse forebrain. *Dev Biol* **335:** 166–178. doi:10.1016/j.ydbio.2009.08.023

Szmyd R, Niska-Blakie J, Diril MK, Renck Nunes P, Tzelepis K, Lacroix A, van Hul N, Deng L-W, Matos J, Dreesen O, et al. 2019. Premature activation of Cdk1 leads to mitotic events in S phase and embryonic lethality. *Oncogene* **38:** 998–1018. doi:10.1038/s41388-018-0464-0

Taschner M, Lorentzen E. 2016. The intraflagellar transport machinery. *Cold Spring Harb Perspect Biol* **8:** a028092. doi:10.1101/cshperspect.a028092

Tran PV, Haycraft CJ, Besschetnova TY, Turbe-Doan A, Stottmann RW, Herron BJ, Chesebro AL, Qiu H, Scherz PJ, Shah JV, et al. 2008. THM1 negatively modulates mouse sonic hedgehog signal transduction and affects retrograde intraflagellar transport in cilia. *Nat Genet* **40:** 403–410. doi:10.1038/ng.105

Tsang B, Arsenault J, Vernon RM, Lin H, Sonenberg N, Wang L-Y, Bah A, Forman-Kay JD. 2019. Phosphoregulated FMRP phase separation models activity-dependent translation through bidirectional control of mRNA granule formation. *Proc Natl Acad Sci* **116:** 4218–4227. doi:10.1073/pnas.1814385116

Wang L, Dynlacht BD. 2018. The regulation of cilium assembly and disassembly in development and disease. *Development* **145:** dev151407. doi:10.1242/dev.151407

Wang J, Garancher A, Ramaswamy V, Wechsler-Reya RJ. 2018. Medulloblastoma: from molecular subgroups to molecular targeted therapies. *Annu Rev Neurosci* **41:** 207–232. doi:10.1146/annurev-neuro-070815-013838

Wang W, Furneaux H, Cheng H, Caldwell MC, Hutter D, Liu Y, Holbrook N, Gorospe M. 2000. Hur regulates p21 mRNA stabilization by UV light. *Mol Cell Biol* **20:** 760–769. doi:10.1128/MCB.20.3.760-769.2000

Wong SY, Seol AD, So P-L, Ermilov AN, Bichakjian CK, Epstein EH Jr, Dlugosz AA, Reiter JF. 2009. Primary cilia can both mediate and suppress Hedgehog pathway-dependent tumorigenesis. *Nat Med* **15:** 1055–1061. doi:10.1038/nm.2011

Yang Y, Roine N, Mäkelä TP. 2013. CCRK depletion inhibits glioblastoma cell proliferation in a cilium-dependent manner. *EMBO Rep* **14:** 741–747. doi:10.1038/embor.2013.80

Zhao X, Pak E, Ornell KJ, Pazyra-Murphy MF, MacKenzie EL, Chadwick EJ, Ponomaryov T, Kelleher JF, Segal RA. 2017. A transposon screen identifies loss of primary cilia as a mechanism of resistance to SMO inhibitors. *Cancer Discov* **7:** 1436–1449. doi:10.1158/2159-8290.CD-17-0281